ICAS 2020 SHANG HAI
International Council of the Aeronautical Sciences
32nd Congress of the International Council of the Aeronautical Sciences
September 6-10, 2021
Pudong Shangri-La, Shanghai, China

EXPERIMENTAL INVESTIGATION AND LIFE PREDICTION FOR DE-FECT INDUCED CRACK OF A P/M NICKEL BASED SUPERALLOY

SHI Yi[1,2*], YANG Xiaoguang[1], SHI Duoqi[1], YANG Didi[1] , MIAO Guolei[3]&LV Shuangqi[4]

[1]School of Energy and Power Engineering, Beihang University, China 100191

[2]School of Materials Science and Engineering, Shanghai Jiao Tong University, China 200240

[3] Chengdu Holy Industry & Commerce Corp. LTD, Chengdu, China

[4]Aviation Engineering Institute, Civil Aviation Flight University of China, China 618307

Abstract

This paper presents the effect of natural and artificial defects on fatigue life of FGH96 at 600℃. The artificial defects were machined by EDM (electron discharge maching) technique. First the fractography of specimens were examined by SEM to obtain defect size and analyse the failure process. Since defects were the fatigue source and a fracture mechanic-based life prediction model was proposed. The shape of natural defects is irregular and the concept of effective area proposed by Murakami was applied. The corresponding maximum K calculation was modified by considering the influence of shape ratio. The small crack growth behaviour was also considered and by integrating the rate equation with initial defect size, and good life prediction was obtained for both two kinds of surface defect.

Keywords: nickel-based superalloy, fatigue life, defect, life prediction, small crack

1. Introduction

Powder metallurgy (P/M) nickel-based superalloys are employed for turbine discs of advanced aero-engines due to its excellent mechanical properties at elevated temperature. Since turbine discs are fracture-critical components, understanding the residual life under working conditions is necessary for safety operation. By now, many researches focused on the fatigue life, creep-fatigue, fatigue crack initiation and growth behaviour for P/M material [1–5]. However, these studies do not include the existence of inclusions and treat material as homogenous. Actually, the material is not so ‘perfect’ and defects (e.g. inclusions and pores) are inevitable in the process of manufacturing and machining. The existence of inclusion changes local material property and results in premature crack nucleation in early stage. It is also found that inclusion dominantly controls the number of cycles to form a crack and fatigue life [6].

In addition, the existence of defects induces local stress concentration. However, the traditional fatigue theory established on the assumption of flawless material cannot solve this case. Actually, defects consume fewer cycles to form crack and propagate com-pared with perfect material. Thus, a fracture-mechanic based model is proposed. Some researchers have applied fracture-mechanic based model in titanium and aluminum alloy at room temperature [7,8], but the application on nickel-based superalloy at high temperature is little. Therefore, in this study we first investigated fatigue life of FGH96 at high temperature with different defects: natural and artificial. Then we analysed the fractography to provide essential input information for the model. Finally, we developed a fracture-mechanic based life prediction method to evaluate the detrimental effect of different defects. In addition, the small crack stage was included in the model.

2. Material and experiment

2.1 Material and test specimens

FGH96 is a P/M nickel-based superalloy named and the typical chemical composition is presented in Table 1. The material was subjected to the following heat treatment: 1140~1150℃/2 h → oil quenching→ 760◦C /8 h and AC (AC: air cooling) before machined. The yield and ultimate tensile strength of this material at 600℃ are about 1030MPa and 1500 MPa, respectively.

The geometry of test specimens is shown in Figure. 1. There are two groups of test specimens: smooth specimens and specimens with surface artificial defects. The defects were obtained by the Electrical Discharge Machining (EDM) technique. Two kinds of defect size were employed with a=200 and 400μm depth notch. The schematic of the artificial defect is shown in Figure. 2.

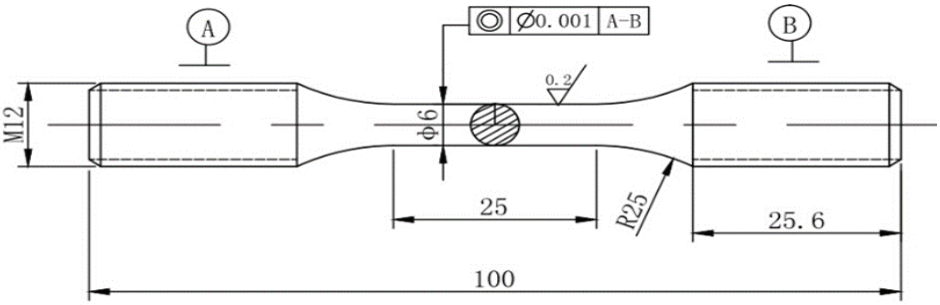

Figure. 1 The geometry of the fatigue specimen (Unit: mm).

2.2 Experimental procedure

All specimens' surfaces were first grinded by abrasive paper and then electron-polished. Details of the pre-test processes were introduced in our previous work [9]. The purpose of these actions is to produce a "nominally-uniform" surface condition and minimize the effect of residual stress. 7 specimens were manufactured by EDM technique to obtain the surface defects.

The fatigue tests were conducted in a closed-loop SHIMADZU servo-hydraulic testing machine at 600°C in air. Considering the fact that the highest temperature of a certain type turbine disc was approximately 600°C, the testing temperature was set at 600°C. Tests were conducted in load control conditions using a sinusoidal waveform loading at the frequency of 5 Hz. The stress ratio was set at 0.05 and four maximum stress levels (900, 1000, 1100 and 1200 MPa) were chosen for tests. Tests were terminated when the fatigue specimens fractured. The stress levels were set based on the stress distribution of one turbine disc at some typical positions such as turbine disc bore, rim and mortises.

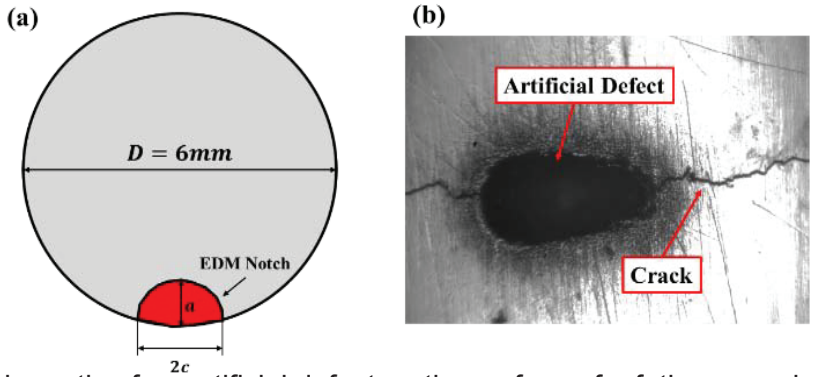

Figure. 2 (a) The schematic of an artificial defect on the surface of a fatigue specimen; (b) The surface defect observed by microscope at room temperature.

3. Results and analysis

3.1 3.1 Fatigue life results

3.1.1 *Smooth specimen*

For smooth specimens, the number of test specimens are different in each stress level, to obtain more types of failure location and source. Eventually, the number of specimens for 900, 1000, 1100 and 1200 MPa is 6, 12, 8 and 7, respectively. All the smooth specimens were examined by SEM observation to identify the location and type of fatigue source. The locations of fatigue source are categorized into three kinds: i) surface; ii) sub-surface; iii) internal. Meanwhile, there are two types of fatigue sources: i) facet; ii) inclusion. Since the purpose of this study is to investigate failures caused by defects, all cracks initiated from inclusions regardless of their location were chosen as the main results.

Figure. 3(a) shows the fatigue test result of smooth specimens with solid points. The light black symbols indicate the failure caused by facets regardless of locations. There are total 8 fatigue specimens of which crack initiated by inclusion. At higher stress level, inclusions initiated at surface. With the decrease of σ_max, the position of failure source transferred from surface to sub-surface and inner place. From the perspective of long and short life, surface inclusion exhibits the worst life. This is especially obvious when σ_max is 1200 MPa. At that stress level, the life of inclusion specimens was only one-fifth of facets. However, the detrimental effect of inclusions is reduced at lower stress level. Sub-surface and internal inclusions have longer life than some facet specimens at the identical stress level. Overall, inclusions exhibit shorter life than the mean live of each stress level and surface defect is the most detrimental one compared with sub-surface and inner position.

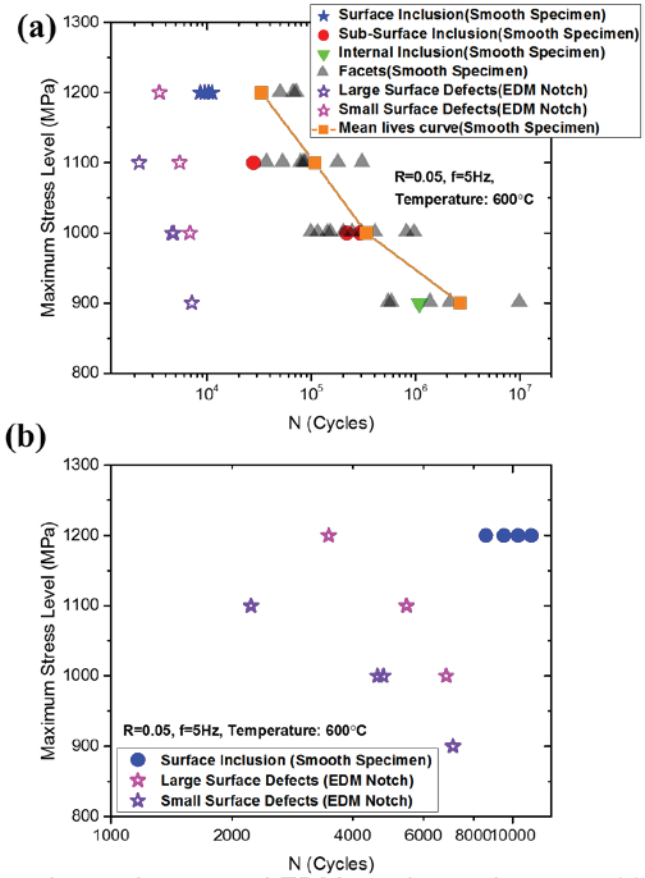

Figure. 3 Fatigue life of smooth specimens and EDM notch specimens at 600◦C: a) all specimens; b) only surface defects.

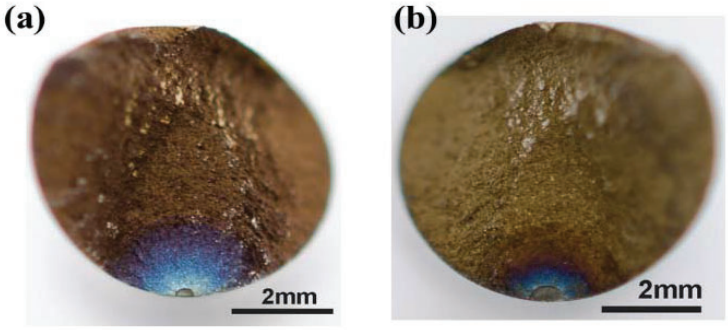

Figure. 4 The macro-fractography of EDM notch specimens: a) small surface defect; b) large surface defect.

3.1.2 EDM notch specimens

There are seven EDM notch specimens tested at elevated temperature. For three small surface defects, with depth a=200μm and width 2c=400μm, stress level ranges from 1000 to 1200MPa. For four large surface defects, with depth a=400μm and width 2c=800μm, stress level ranges from 900 to 1100 MPa. Test results of EDM notch specimens are shown in Figure. 3(a) with hollow symbols. Obviously, specimens with these artificial defects have shorter fatigue life. And Figure. 3(b) further presents results of artificial defects and smooth specimens. First, the scatter of EDM notch specimens is obviously small compared with that of smooth specimens. In other words, the artificial surface defect limits other factors like facets and the inner inclusions which exhibit longer life. Secondly, the results of EDM show that larger defect has shorter life with the identical maximum stress level. Meanwhile, the artificial defect size is larger than the inclusion size of smooth specimens which will be further introduced in Section 3.2.

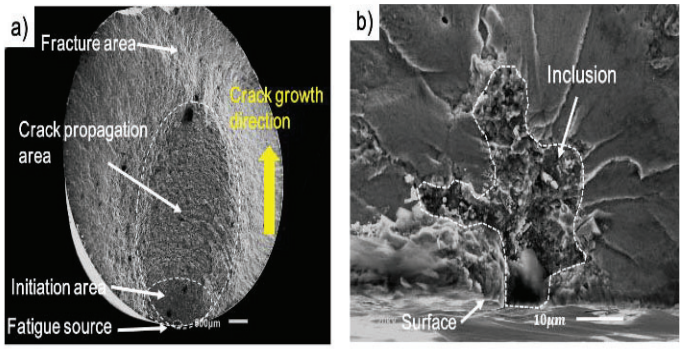

Figure. 5 SEM observation of smooth specimen with surface inclusion: a) the fracture surface; b) the inclusion at the surface.

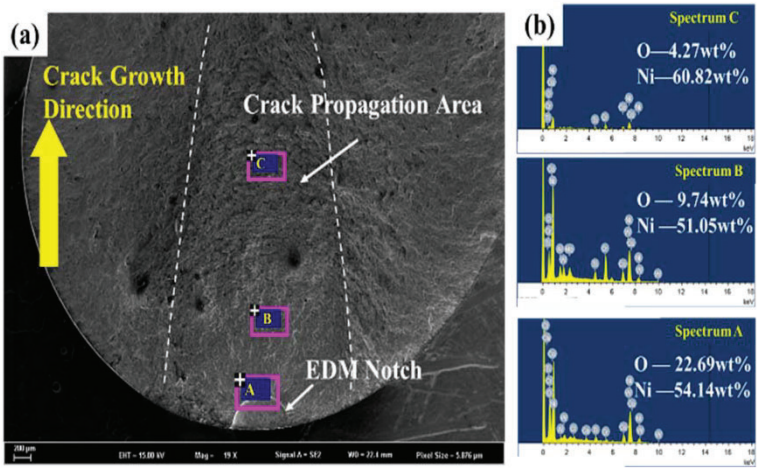

Figure. 6 (a) The SEM observation of fracture surface of EDM notch specimen; (b) The EDS result of three positions.

3.2 Fractography

The macro-fractography of the EDM notch specimens are shown in Figure. 4. The crack front of the notch is approximately an arc. Due to the elevated temperature, the mark of heat tinting can also be observed from Figure. 4. The area of crack initiation and propagation and the final fracture area can also be distinguished. Figure. 5 presents the SEM observation of a smooth specimen. Similarly, different stage of the fatigue process can be identified. The rougher surface represents the fracture area, and the beach marks on the fracture surface indicate the crack growth direction illustrated by the yellow arrow. Figure. 5(b) shows the irregular feature of the inclusion, which is various from the artificial defect. Figure. 6(a) also presents the fracture surface of EDM notch specimen, and the overall beach mark is also similar to the smooth specimen with surface inclusion. Both two types of specimens containing surface defect indicate that most cycles were consumed in the crack propagation stage. Figure. 6(b) shows the EDS result of the EDM notch specimen with different positions. The notch location, denoted as point A in Figure. 6(b) has the highest oxygen element weight percent compared with inner places (point B and point C). The surface defect was exposed to the air environment where oxidation was dominant at elevated temperature. To some extent, sub-surface and internal defect could have longer fatigue life under identical condition since they are isolated from oxidation and have a vacuum-like environment [9]. It has been shown that fatigue crack growth life for specimens tested in vacuum were longer than in air [10]. Considering the engineering application, the worst life is of more interest. Therefore, we put more emphasis on surface defects like inclusions or voids.

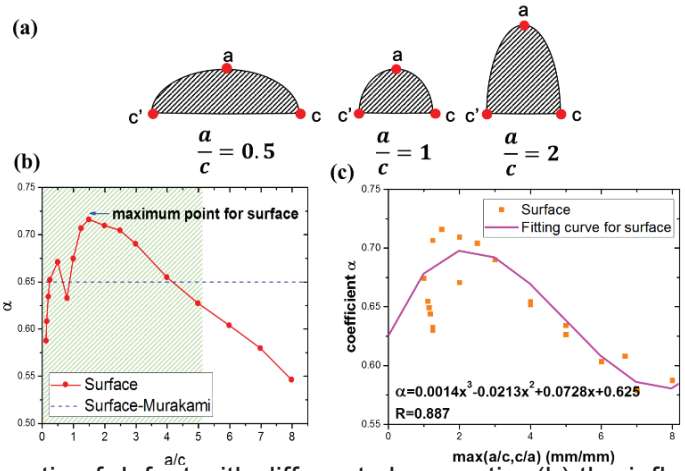

Figure. 7 (a) The schematic of defect with different shape ratio; (b) the influence of shape ratio on coefficient α; (c) the modified curve for new shape ratio;

3.3 Fracture mechanic-based model

Based on the analysis before, since more cycles were consumed in the crack propagation stage, it is reasonable to propose a fracture mechanic-based model.

3.3.1 The stress intensity calculation

Stress intensity factor (SIF) is widely used to characterize the stress filed at the crack tip under the framework of linear elastic fracture mechanic (LEFM). For I mode crack propagation, SIF is often denoted as K_I and is expressed in Equation (1).

$$K_I = Y\sigma\sqrt{\pi a} \tag{1}$$

where Y is the geometry factor; σ is nominal stress; a is the crack length. The commonly-used unit of SIF is $\mathrm{MPa}\sqrt{m}$. Generally, SIF equation is related to a wide range of configuration parameters, such as parametric angle, crack depth, crack length, plate thickness and width. However, Murakami proposed '$\sqrt{\mathrm{area}}$' as a new promising geometrical parameter for SIF calculation neglecting the specimen geometry, shown in Equation(2)(3)[11,12].

$$K_{Imax\_internal} = 0.5\sigma\sqrt{\pi\sqrt{area}} \tag{2}$$

$$K_{Imax\_surface} = 0.65\sigma\sqrt{\pi\sqrt{area}} \tag{3}$$

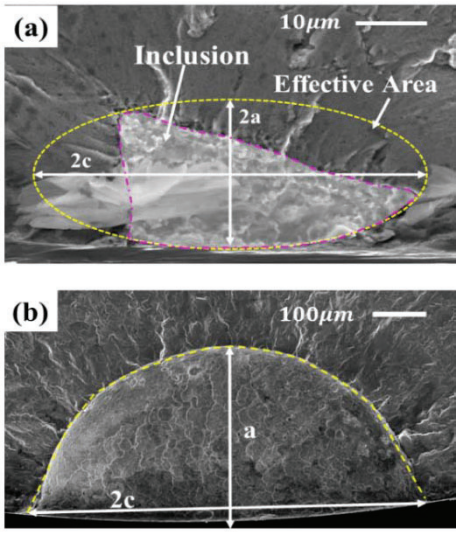

Figure. 8 The effective area for surface defects: (a) surface natural inclusion; (b) artificial surface de-fect.

These equations provide a simpler approximation method for SIF calculation and also emphasizes on the maximum of SIF. Actually, the SIF of each point along the crack tip is different and usually the maximum SIF point is the interest of the study. For example, as shown in Figure.7(a), for a/c=1, all point A, C and C' have the same K value. For a/c< 1, the maximum K point is point A, while for a/c>1, the counterpart is point C and C'. Combing the Eq.(2)(3), the expression of maximum K value can be written in:

$$K_{Imax} = \alpha\sigma\sqrt{\pi\sqrt{area}} \tag{4}$$

However, Murakami directly specified the value of α, but it is still doubtful whether the shape ratio will influence the value. Figure. 7 (b) shows the coefficient α is dependent on the shape ratio. Solid points in Figure. 7(b) and (c) were generated by Nasgro software SC30 case. The constant coefficient provided by Murakami could provide an accuracy of 10% in LEFM range[13]. In Figure. 7(c), when shape ratio equals 1, the coefficient reaches the minimum point for both internal and surface crack case and it appears to be a symmetry point. Therefore, we re-plotted the Figure. by using the new value $\max(a/c, c/a)$, shown in Figure. 7(c). The influence of shape ratio could be expressed in polynomial form with 0.88 regression coefficient.

For smooth specimen with natural inclusion, the maximum K value is calculated based on the concept of equivalence. Murakami[12] first proposed to use an effective area which is estimated by considering a smooth contour enveloping the original irregular shape. Yadollahi et al.[14] replaced a real irregular flaw with an equivalent smooth-shaped crack in investigating the effect of process-induced voids on fatigue life of an additively manufactured material. In their work, the influence of small local curvature is limited but another geometry parameter: overall aspect ratio would be important. For the EDM notch specimen, the shape of crack front is relatively regular. Therefore, these defects sizes are measured directly without applying the concept of equivalence. However, it is worth mentioning, for inclusion of smooth specimen, the defect is replaced with a ellipse, while for EDM notch specimen, the defect shape is a semi-ellipse, shown in Figure. 8 and detailed sizes are listed in Table 1

3.3.2 Small crack modification

A typical crack propagation consists of three stages, shown in Figure. 9. The II stage represents the steady crack propagation which is usually described by Paris equation. III stage is a rapid propagation stage which is close to fracture. It is generally accepted that when SIF is smaller than the threshold value ΔK_{th}, the crack would not grow. However, the existence of small crack violates this concept, which grows at the SIF below the threshold value and has higher growth rate. In Figure. 9, the blue dash line represents the Paris equation. However, when it extends to stage I and III, Paris equation is invalid. The ignorance of small-crack effect results in non-conservative life prediction. Therefore, modification should be introduced to describe the 'abnormal' small crack growth behavior.

Many researchers used the crack closure theory to interpret the anomalous behavior and introduced

effective SIF into the crack growth rate equation[15–17]. Meanwhile, the threshold value for small crack stage is also influenced by the crack length[8,18]. At the beginning of loading, the plastic zone is small and just ahead of the initial crack. With the increase of cycles, the size of plastic zone and crack length increase simultaneously.

If most of cracks are surrounded by plastic zone, the crack could arrest due to the plasticity-induced crack closure. Whereas, if the increment of plastic zone falls behind the growth of SIF, the crack will go forward. Therefore, the crack threshold value in small crack stage is relevant to the crack length. Many other studies[16,19,20] also mentioned the relationship between crack length and threshold, shown in Equation (5) and Figure. 10, and U.Zerbst[21] rewrote it in the form of $\sqrt{area}$.

$$\Delta K_{th} = \Delta K_{in} + \Delta K_{ex} = \Delta K_{in} + \left(\Delta K_{th_{long}} - \Delta K_{in}\right) \cdot [1 - e^{-k(a-D)}] \tag{5}$$

Where $\mathrm{k} = \frac{1}{4D}\frac{\Delta K_{in}}{\Delta K_{th_{long}} - \Delta K_{in}}$ is a material relevant coefficient, D represents the average microstructural dimension. The ΔK_{th} consists of two parts: 1) the intrinsic threshold is determined by microstructure and independent of loading; 2) the extrinsic threshold is related to plasticity-induced crack closure and influenced by stress ratio, environment, etc. The crack initiation in Figure. 10 means the crack grows within a grain, where LEFM is inappropriate. If the external loading is small, whose corresponding SIF range doesn't exceed the ΔK_{th}, the crack would not propagate, as shown case S1. For case S2, although the ΔK value is large enough at initial, the threshold value then is larger than the applied one. Therefore, the crack arrest, as the S1 case shown in Figure. 9. In other words, with the progress of loadings, more plasticity is accumulated at the crack tip. If the crack growth driving force is less than the residual plasticity induced resistance, the crack arrests. Therefore, the effective driving force is written as Eq.(6) and shown as the case S3 in Figure. 10.

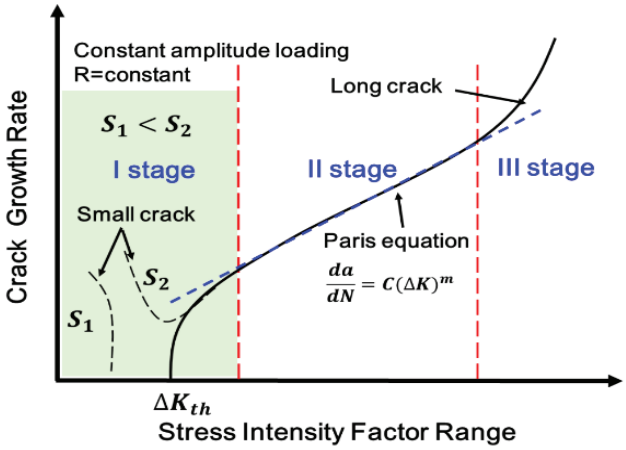

Figure. 9 The schematic of a typical small and long crack propagation.

$$\Delta K_{eff} = \Delta K_{app} - \Delta K_{th} \tag{6}$$

This could also explain the abnormal behaviour of small crack in Figure. 10 because the nominal ΔK does not reflect the reduction of real crack driving force in small crack stage. For example, in S3 case the ΔK_{eff} first decreases and then increases because the curve of ΔK_{th} is convex. Meanwhile, for shorter crack length, the value of ΔK_{app} and ΔK_{th} both increase. Once the crack length reaches certain level, the ΔK_{th} stabilizes at the value of ΔK_{th_long}. For long crack, the plastic zone at the crack tip is relatively small compared with the crack length.

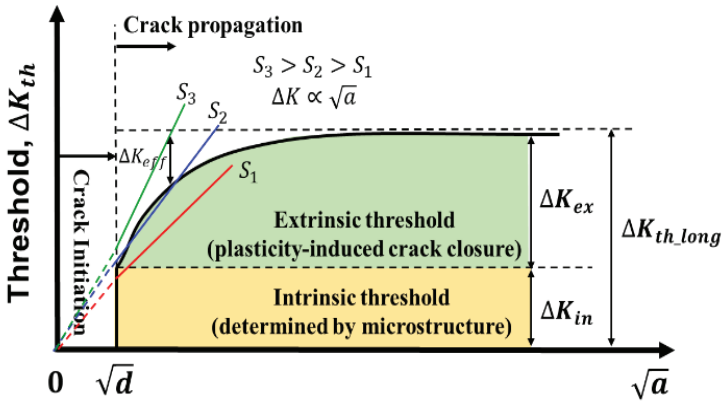

Figure. 10 The composition of crack threshold value.

3.3.3 *Fatigue life model*

The fatigue life is calculated by integrating the fatigue crack growth rate (FCGR) equation with initial and final value. The FCGR equation consists of two parts. For small crack, the FCGR equation is based on NASGRO equation. Here, we mainly consider the initial part and the denominator part indicating the third stage is neglected, shown in Eq.(7).

$$\frac{da}{dN} = C(\Delta K_{eff})^n (1 - \frac{\Delta K_{th}}{\Delta K})^p \tag{7}$$

For the long crack part, we directly apply the Paris equation, shown in Eq.(8).

$$\frac{da}{dN} = C(\Delta K)^n \tag{8}$$

Meanwhile, in this study, the crack is a two-dimensional crack instead of a through crack which is a one-dimensional crack. Therefore, the crack length term a in Eq.(5) is substituted by $\sqrt{area}$, shown in Eq.(9).

$$\Delta K_{th} = \Delta K_{in} + \Delta K_{ex} = \Delta K_{in} + \left(\Delta K_{th_{long}} - \Delta K_{in}\right) \cdot [1 - e^{-k(\sqrt{area}-D)}] \tag{9}$$

The size of the inclusion could easily obtain from the fractography. In addition, the material related parameters refer to the corresponding material handbook and related studies. The stage of small crack and long crack is distinguished by the long crack threshold value. The terminated condition is set based on the fracture criteria and strength criteria. If the residual strength or the maximum K value exceeds the critical value, then the integration ends. These two criteria play the role of final value in integration calculation. The flowchart of the above-mentioned model is shown in Figure. 11 and the relevant input parameters are listed in Table 3. In Figure. 11, the green rectangular represents the small crack stage while the blue one represents the long crack stage. The main difference between them is the FCGR equation and the driving force. Most material and FCGR relevant parameters refers to the report [22]. The FCG tests were conducted at 600◦C at the frequency of 5Hz. It is also worth mentioning that some parameters were obtained by trial method due to the insufficient published data. However, these values also belong to the reasonable range.

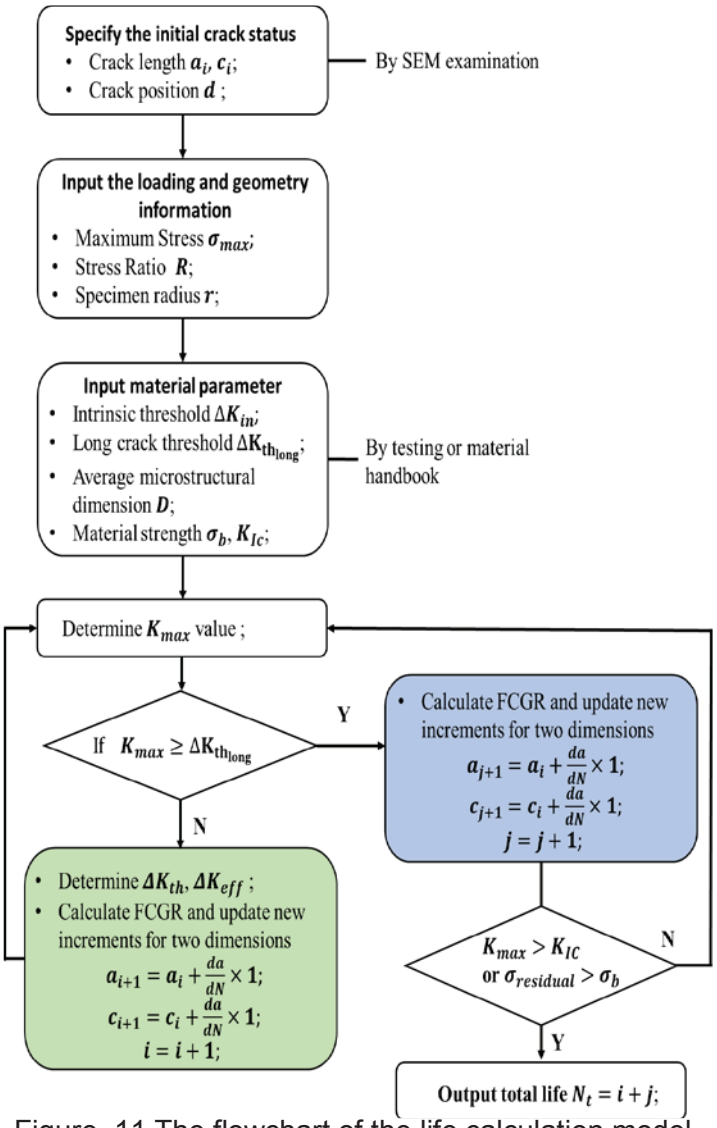

Figure. 11 The flowchart of the life calculation model.

The comparison between the predicted and experimental life is shown in Figure. 12. This fracture-mechanic based life prediction model generates good life prediction. The black lines indicate the ± 2 times band and all points fall into this band. Actually most points in Figure. 12 is close to the line with slope equals one. But one large surface defect point presents non-conservative prediction obviously. Figure. 13 shows the proportion of long and short crack of all test specimens. Obviously, smooth specimens have around 10%-25% small crack proportion. While for EDM notch specimen, none stage is consumed in small crack stage. This is mainly due to the initial crack size, since the artificial notch size is larger than that of natural inclusions. For smooth specimen, their initial SIF value is below the threshold value while for artificial specimen is vice versa. According to the classical theory, if the initial SIF value is lower than the threshold value, crack will not propagate. However, actually the crack in smooth specimen grows and the corresponding fatigue life is shorter than traditional expectation. Table 2 lists all initial defect size of smooth and EDM machined specimens and it ranges from approximately 18 to 400μm in depth (an order's difference). However, their corresponding life difference is smaller than the geometry size. When these sizes are input into the maximum SIF calculation, their difference including loading is evaluated by the crack growth driving force. Combined with the result, applying fracture mechanic model to describe the fatigue process is reasonable.

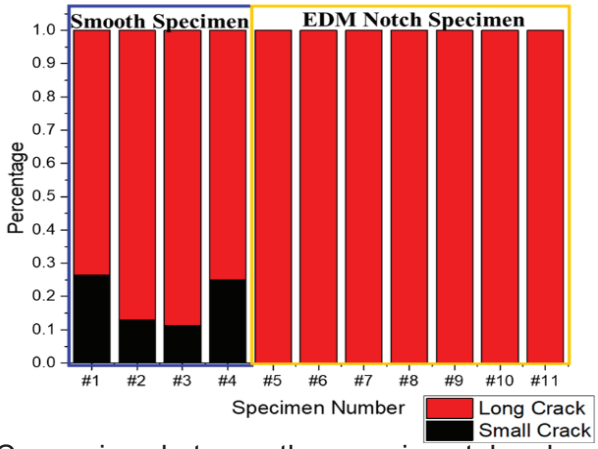

Figure. 12 Comparison between the experimental and predicted life.

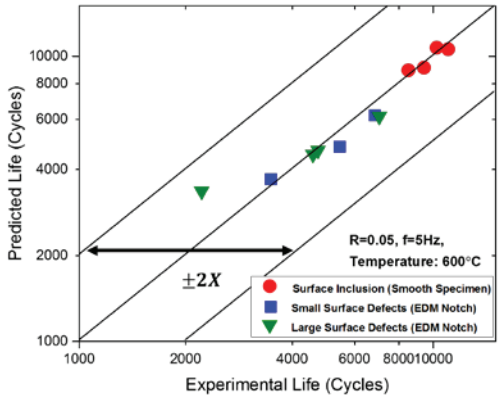

Figure. 13 The proportion of small and long crack stage of all specimens.

4. Conclusions

A fracture mechanic-based life prediction model was proposed in this paper. The model was also validated by the experimental results of natural and artificial defects. The conclusions are drawn below:

(1) Both natural and artificial defects can be the fatigue source and limit fatigue life. The fractography shows three distinct area: initiation, propagation and fracture area. And based on these, a life prediction model based on fracture-mechanics was proposed.

(2) To apply the fracture mechanics, the irregular shape of natural defect is dealt with by applying the effective area. And the Murakami maximum K value equation is modified by considering the influence of shape.

(3) The small crack effect is included in the life model. The driving force in this stage is modified with the changing threshold value which is the function of crack length. For inclusions with smaller initial K value, more cycles are consumed in small crack stage. However, inclusions with large initial K value, more cycles are consumed in long crack stage.

(4) The life prediction model generates good prediction for two kinds of defects, and all points fall into a ±2 times error band.

Acknowledgment – This research is sponsored by the National Natural Science Foundation of China (No. 51775019) and the National Science and Technology Major Project (2017-IV-0012-0049). The author would also express gratitude to Mr. CAI Y.H.(Beijing Institute of Electro-Machining) and Mr. ZHOU Y.D, Mr. MIAO Y. and Mr. HUANG J. et al. (Shanghai Aeronautical Materials & Structures Testing Co.,LTD)'s support in fatigue tests.

*Corresponding author: Dr. SHI Yi
E-mail address: shiyi_sepe@sjtu.edu.cn

References

[1] Chen SY and Wei DS, Mater Sci Eng A, Vol.749, pp 106–117,2019.
[2] Yang H and Bao R, Int J Fatigue, Vol.33, pp 632–641,2011.
[3] Na S and Yoon D, Int J Fatigue,Vol.101,pp 27–35,2017.
[4] Knowles DM and Hunt DW. Metal Mater Trans A Phys Metall Mater Sci, Vol. 33, pp 3165–3172,2002.
[5] Jiang R and Pierron F, Mater Sci Eng A, Vol. 699, pp 28–44,2017.
[6] McDowell DL and Dunne FPE. Int J Fatigue, Vol. 32, pp 1521–42,2010.
[7] Léopold G and Nadot Y, Fatigue Fract Eng Mater Struct, Vol. 38, pp 1026–41,2015.
[8] Zerbst U and Madia M, Eng Fail Anal, Vol. 97, pp 777–792,2019.
[9] Miao G and Yang X, Mater Sci Eng A, Vol. 668, pp 66–72,2016.
[10]Cashman GT. Int J Fatigue, Vol. 32, pp 492–496,2010.
[11]Murakami Y and Usuki H. Int J Fatigue, Vol. 11, pp 299–307,1989.
[12]Murakami Y. Metal Fatigue:Effects of small defects and nonmetallic inclusions. Elsevier; 2002.
[13]McEvily AJ and Endo M, Fatigue Fract Eng Mater Struct, Vol. 26, pp 269–278, 2003.
[14]Yadollahi A and Mahtabi MJ, Fatigue Fract Eng Mater Struct, Vol. 41, pp 1602–14, 2018.
[15]Sadananda K and Nani Babu M, Mater Sci Eng A, Vol. 754, pp 674–701, 2019.
[16]Maierhofer J and Pippan R, Int J Fatigue, Vol. 59, pp 200–7, 2014.
[17]Endo M and McEvily AJ. Mater Sci Eng A, Vol. 468–470, pp 51–58, 2007.
[18]Chapetti MD. Int J Fatigue, Vol. 25, pp 1319–1326, 2003.
[19]Chapetti MD and Steimbreger C. Int J Fatigue, Vol. 125, pp 23–34, 2019.
[20]Wu SC and Xu ZW Int J Fatigue, Vol.103, pp 185–95, 2017.
[21]Zerbst U and Madia M, Eng Fract Mech, Vol. 82, pp 115–34, 2012.
[22]Beijing Institute of Aeronautical Materials. FGH96 Fatigue Crack Growth Test Report. 2016.

Table 1. Nominal chemical compositions of FGH96 (wt. %).

Ni	C	Cr	Co	W	Mo	Ce
Bal	0.02~0.05	15.50~16.50	12.50~13.50	3.80~4.20	3.80~4.20	0.01
Al	Ti	Zr	Nb	P	B	S
2.00~2.40	3.50~3.90	0.025~0.050	0.50~1.00	0.015	0.060~0.015	0.015

Table 2. Detailed result of the surface defect specimens.

Specimen	Defect type	No	σ_{max}(MPa)	Cycles	$2a_i$(μm)*	$2c_i$(μm)	$\sqrt{area_i}$(μm)
Smooth Specimen	Natural Defect-Surface Inclusion	#1	1200	8581	53.81	34.61	38.24
		#2	1200	9504	42.83	44.70	38.77
		#3	1200	10322	17.94	49	26.27
		#4	1200	11119	34.76	33.73	30.34
EDM-Notch Specimen	Small Surface Defect	#5	1200	3482	204	422	342.91
		#6	1100	5443	208	376	326.84
		#7	1000	6832	196	404	328.87
	Large Surface Defect	#8	1100	2230	397	820	666.83
		#9	1000	4609	377	778	632.95
		#10	900	7101	344	750	593.64
		#11	1000	4763	351	736	594.02

*For EDM Notch Specimen, the value is a_i(μm)

Table 3. The relevant input parameters for life model of FGH96.

Types	Parameters	Value	Unit	Remarks
Small crack relevant parameters	$\Delta K_{th_{long}}$	8	MPa$\sqrt{m}$	Refer to [22]
	ΔK_{in}	1.9	MPa$\sqrt{m}$	Trial
	D	23	μm	Generated by our previous EBSD analysis[9]
FCGR equation relevant parameters	p	0.5	/	Trial
	n	2.28	/	Refer to [22]
	C	1E-7		Refer to [22]
Material Strength	σ_y	1030	MPa	FGH96 at 600°C
	σ_b	1500	MPa	FGH96 at 600°C
Fracture Toughness	K_{IC}	60	MPa$\sqrt{m}$	Refer to [22]